Available online at www.sciencedirect.com

SciVerse ScienceDirect

Nuclear Medicine and Biology 39 (2012) 167–176

NUCLEAR MEDICINE — AND — BIOLOGY

www.elsevier.com/locate/nucmedbio

Synthesis and evaluation of [^{18}F]exendin (9–39) as a potential biomarker to measure pancreatic β-cell mass

Yi Wang[a,c], Keunpoong Lim[a], Marc Normandin[a], Xiaojian Zhao[b], Gary W. Cline[b], Yu-Shin Ding[a,*]

[a]*Department of Diagnostic Radiology, Yale University School of Medicine, New Haven, CT 06520, USA*
[b]*Department of Internal Medicine, Yale University School of Medicine, New Haven, CT 06520, USA*
[c]*School of Environment, Tsinghua University, Beijing 100084, P.R. China*

Received 19 December 2010; received in revised form 24 June 2011; accepted 15 July 2011

Abstract

Introduction: Glucagon-like peptide 1 (GLP-1) is released in response to food intake and plays an important role in maintaining blood glucose homeostasis. Exendin (9–39), a potent glucagon-like peptide 1 receptor antagonist, has been labeled with In-111 for SPECT imaging. We report here the first radiosynthesis of [^{18}F]exendin (9–39) ([^{18}F]Ex(9–39)) and an evaluation of its potential as a biomarker for in vivo positron emission tomography (PET) imaging of pancreatic β-cell mass (BCM) in rats.

Methods: F-18 label was introduced by conjugation of [^{18}F]4-fluorobenzaldehyde with an Ex(9–39) derivative containing a 6-hydrazinonicotinyl group on the ε-amine of Lys27. Positron emission tomography imaging was carried out in Sprague–Dawley rats (five control and five streptozotocin-induced diabetic) and BioBreeding diabetes-prone rats (three at 7 weeks and three at 12 weeks) using the high-resolution research tomograph (HRRT) after 0.187±0.084 mCi [^{18}F]Ex(9–39) administration. Time–activity curves were obtained from pancreas, liver and kidney. Pancreases were assayed for insulin content after the imaging study.

Results: Site-specifically labeled [^{18}F]Ex(9–39) was purified on a G15 open column with radiochemical and chemical purities >98%. Positron emission tomography imaging showed pancreatic standardized uptake value (SUV) peaked at 10 min and plateaued by 50 min to the end of scan (240 min). No correlations of pancreatic SUV with postmortem measures of insulin content were seen.

Conclusions: [^{18}F]Ex(9–39) was successfully prepared and used for PET imaging for the first time to measure pancreatic BCM. The results suggest that derivatization of the Lys27 residue might reduce binding affinity, as evidenced by the absence of specific binding. Exendin analogues radiolabeled at other sites may elucidate the active site required for binding.

Keywords: Glucagon-like peptide 1 (GLP-1); HYNIC; PET imaging; [^{18}F]Exendin (9–39); Pancreatic β-cell mass; Diabetes

1. Introduction

Glucagon-like peptide 1 receptor (GLP-1R) has recently been shown to be overexpressed in insulinomas, gastrinomas and lung neuroendocrine tumors [1,2], which makes it a promising target for diagnostic and therapeutic purposes, particularly for insulinoma treatment. The endogenous ligand, GLP-1, is ineffective both as an imaging and therapeutic agent because it has a very short half-life (1–2 min) in vivo [3] due to fast degradation by the enzyme dipeptidyl peptidase 4 [4]. Exendin-4, a 39-amino acid peptide hormone found in the saliva of the Gila monster [5], is an agonist of GLP-1R. Exendin-4 has only 53% homology with GLP-1, which increases its resistance to degradation by dipeptidyl peptidase 4 and therefore extends its half-life in vivo to about 2.4 h [6,7]. Exendin-4 has a high affinity to GLP-1R, with a K_d value of approximately 1.4×10^{-10} M [8]. Exendin-4 has been radiolabeled with SPECT imaging radionuclides, such as In-111, and was used to image insulinomas in animals [9,10] as well as in humans [11,12]. Exendin-4 was also radiolabeled with Ga-68 for positron emission tomography (PET) imaging studies [13]. Exendin (9–39) is a truncated version of exendin-4 and also has a high affinity to GLP-1R, with a K_d value of around 3×10^{-9}

* Corresponding author. Tel.: +1 203 785 4297; fax: +1 203 785 3107.
E-mail address: yu-shin.ding@yale.edu (Y.-S. Ding).

0969-8051/$ – see front matter © 2012 Elsevier Inc. All rights reserved.
doi:10.1016/j.nucmedbio.2011.07.011

M [8]. However, unlike exendin-4, truncated exendin (9–39) does not promote the secretion of insulin; instead, it acts as antagonist of GLP-1R and is potentially a competitive inhibitor of exendin-4 [14]. Based on its high affinity to GLP-1R, exendin (9–39) was also labeled with a radionuclide to image the GLP-1R [15].

Our research focuses on identification and evaluation of radiolabeled ligands that bind specifically to molecular targets, allowing for noninvasive in vivo PET imaging of pancreatic islet β-cell mass (BCM). A challenge for imaging BCM is the accumulation of the radioligands by the surrounding organs that can compromise the accuracy of quantitative imaging. Based on database and immunohistochemistry screening, we identified G-protein-coupled receptors (GPCRs), including GLP-1R, which are expressed with a high degree of specificity to islet β-cells for further in vitro and in vivo evaluation for PET imaging of BCM. Immunohistochemical staining of GLP-1R with GLP-1R and insulin antibodies showed colocalization of insulin with GLP-1R. We have also assessed binding and uptake of ^{125}I-exendin (9–39) (PerkinElmer, Boston, MA) to a rat insulinoma β-cell line (INS-1 832/13) and a human pancreatic exocrine cell line (PANC-1) and found a preferential binding of exendin (9–39) to rat insulinoma cells (INS-1) and rat islets in comparison to exocrine cells (PANC-1) [16] (see Sections 2 and 3 for brief experimental procedures and results, respectively). The high expression and specificity of GLP-1Rs on islet β-cells makes it an attractive target for molecular imaging using radiolabeled analogues of exendin-4 [10,17]. Recently, we have shown the feasibility of fluorescent analogues of exendin-4 to image pancreatic islet BCM in vivo. In this study, exendin-4 was conjugated to the monofunctional dye Cy5.5 and the saturation binding was assessed using the INS-1 rat insulinoma cell line. The preferential localization of exendin-4-Cy5.5 to the pancreas was confirmed both in vivo and ex vivo [18] (see Sections 2 and 3 for brief experimental procedures and results, respectively). Furthermore, an ^{111}In-labeled exendin-4 analogue, [Lys40 (Ahx-DTPA-^{111}In)NH_2]exendin-4, has been synthesized and showed high specificity and affinity in targeting GLP-1R with negligible specific and nonspecific binding to surrounding tissue (i.e., liver, stomach, intestines) [10,17]. We hypothesize that ^{18}F-labeled exendin (9–39) can be used to specifically target GLP-1R in β-cells with low surrounding tissue accumulations, allowing for quantitative PET imaging of pancreatic BCM.

To the best of our knowledge, Kimura et al. [19] reported the synthesis of [^{18}F]Ex(9–39) via N-succinimidyl 4-[^{18}F] fluorobenzoate ([^{18}F]SFB). [^{18}F]SFB is an excellent reagent to label peptides with F-18; however, it is not site-specific since the active succinimidyl ester can react with any primary amine group within the peptide molecule. That is, the labeled peptide is a mixture of peptide molecules tagged with [^{18}F]fluorobenzyl groups ([^{18}F]FB) on different amino acid residues possessing primary amine groups. Usually, the amine groups in a peptide molecule are critical to its biological function; thus, an improper introduction of a labeling tag to a critical amine group may result in a loss of the biological activity of the labeled peptide. The modification on the ε-amine of Lys27 has been reported to have minor influence on the binding affinity of the peptide to GLP-1R [20–22]; therefore, in the current work, F-18 label was introduced in a site-specific manner by conjugation of [^{18}F]4-fluorobenzaldehyde ([^{18}F]FBA)with an exendin derivative containing a 6-hydrazinonicotinyl (HYNIC) group on the ε-amine of Lys27 through the formation of a hydrazone. Small-animal PET imaging was carried out in Sprague–Dawley (SD) rats and BioBreeding diabetes-prone (BB-DP) rats following administration of [^{18}F]Ex(9–39). Time–activity curves (TACs) were obtained for pancreas, liver and kidney. The pancreases were assayed for insulin content after sacrificing the animals at the end of PET scans. Data were examined for correlations between uptake of tracer in pancreas measured by PET and islet insulin expression measured by postmortem histology.

2. Methods and materials

The β-cell selectivity of exendin and its analogues were evaluated via in vitro and in vivo tests before the PET imaging studies with F-18-labeled exendin.

2.1. β-Cell selectivity: in vitro cell binding assays

We assessed binding and uptake of ^{125}I-exendin (9–39) (PerkinElmer) to a rat insulinoma β-cell line (INS-1 832/13) and a human pancreatic exocrine cell line (PANC-1) [23]. Briefly, INS-1 cells, islets or PANC-1 cells were preincubated in Krebs–Ringer buffer (KRB) (3 mM glucose), and "uptake" was assessed after a 30-min incubation with ~4 μCi of ^{125}I-exendin (9–39). Uptake was measured in the cell pellet from the media after oil (*n*-dodecane/bromodocane, 1:37.5) partitioning of the cell pellet from the media and includes both membrane bound and internalized cell associated radioligand activity. Retention was determined after another 30-min incubation in ligand-free media and is the internalized cell associated radioligand activity. Any nonbound radioligand activity in the cell pellets, due to residual extracellular water, was corrected by coincubating the ^{3}H-radioligands with ~2 μCi of [^{14}C]sucrose. The radioactivity in the residual extracellular water was less than 0.7% of the cell-associated radioactivity. Fractional cell associated radioactivity of uptake and retention of the ligands to the cells were normalized to intracellular water space. Intracellular water in the cell pellet was determined in separate incubations of the cells with [^{3}H]water and [^{14}C]sucrose. All determinations were performed in triplicate.

2.2. Molecular targeted fluorescent imaging of pancreatic BCM with exendin-4-Cy.5.5

Exendin-4 (Sigma) was conjugated to the monofunctional dye Cy5.5 (Amersham) using the manufacturer's recommended protocol to yield a dye-to-protein ratio of ~0.4:1. Saturation binding was assessed using the INS-1 (832/13) rat insulinoma cell line. Cells were grown to confluence in 96-well plates and incubated with varying concentrations of exendin-4)-Cy5.5 for 1 h in KRB (2.5 mM glucose) and washed with PBS (2×). Fluorescence was measured at 700 nm (excitation 625 nm) using the Kodak Image Station In-Vivo FX multimodel imaging system. The efficacy of targeted imaging of BCM in vivo was evaluated in hairless SKH1 mice using the Image Station equipped with a customized heated chamber. Baseline and sequential 1-min images were collected in the isoflurane-anesthetized mouse following a bolus injection of approximately 40 nmol of exendin-4-Cy5.5 via an indwelling jugular catheter. At the end of the imaging session, mice were euthanized and relative fluorescence intensity was determined on the excised tissues.

2.3. Reagents and instrumentation

All the purchased reagents were used without further purification. Kryptofix 2.2.2. (K_{222}), K_2CO_3, K_2SO_4, 4-fluorobenzaldehyde, aniline, ethanol, ascorbic acid, 2-(*N*-morpholino)ethanesulfonic acid (MES), anhydrous dimethyl sulfoxide (DMSO) and Sephadex G-15 were purchased from Sigma-Aldrich. SPE cartridge Chromafix 30-PS-HCO_3 was purchased from Macherey-Nagel (Germany). Other reagents were obtained from various commercial suppliers. Exendin (9–39) was purchased from 21st Century Biochemicals (Marlboro, MA) with a 6-HYNIC group introduced on the ε-amine on the Lys27. The amino acid sequence of the peptide used in this study was DLSKQMEEEAVRLFIEWL[K-ε-hydrazino]NGGPSSGAPPPS-amide (see Supplemental Information for the analytical sequencing data). A precursor 4-formyl-*N*,*N*,*N*-trimethylanilinium triflate was synthesized in-house according to a method published in the literature [24]. The reversed phase semipreparative Gemini high-performance liquid chromatography (HPLC) column (250×10 mm, 10 μm) was purchased from Phenomenex (Torrance, CA). The mobile phase for preparation of [^{18}F]FBA was 30% acetonitrile (CH_3CN)/70% 0.2% acetic acid at a flow rate was 5 ml/min. The Superdex peptide column was purchased from GE Healthcare (Piscataway, NJ). A Shimadzu LC-20AT Prominence system was used, which is equipped with a SPD-M20A diode array (PDA) detector or SPD-20A UV/Vis detector connected in series with a Bioscan Flow-Count gamma detector. Dual UV wavelengths can be selected and monitored simultaneously after sample injection. For this study, absorbances at 254 and 360 nm were selected. [^{18}F]Fluoride was produced (30 min beam, 35 μA) on a GE PETtrace cyclotron using a $^{18}O(p,n)^{18}F$ reaction in a GE high-yield target assembly.

2.4. Synthesis of 4-formyl-N,N,N-trimethylanilinium triflate

A 250-ml round bottom flask was purged with argon for 10 min. With continued argon purging, 4-*N*,*N*-dimethylaminobenzaldehyde (5.4 g, 36.2 mmol) was added into the flask, followed by addition of anhydrous dichloromethane (120 ml). A clear solution was obtained upon gentle stirring. Under argon atmosphere and with continuous stirring, methyl trifluoromethane sulfonate (8.0 g, 48.7 mmol) was added dropwise via a syringe. After stirring for 8 h, the precipitate was collected by filtration and recrystallized from dichloromethane/diethyl ether to afford 4-formyl-*N*,*N*,*N*-trimethylanilinium triflate as a white powder (7.8 g, 68.8% yield); $C_{11}H_{14}NO_4SF_3$ M=313.29 g/mol. ^{1}H-NMR (d_6-DMSO, 500 MHz): δ3.61 (9H, s), δ8.11–8.18 (4H, m), δ10.07 (1H, s).

2.5. Coupling of FBA to HYNIC-functionalized exendin peptide to prepare the nonradiolabeled test compound, F-19-exendin (9–39) peptide, as the reference

To prepare the nonradiolabeled test compound, i.e., F-19-exendin (9–39) peptide, as the reference and to optimize the reaction conditions for coupling of FBA with HYNIC-functionalized exendin peptide, the coupling reactions were carried out under different conditions. Exendin peptide (30 μg, MW 3505.8, 8.56×10^{-3} μmol) and FBA (1.0 μg, 8.06×10^{-3} μmol) were dissolved in 200 μl of 100 mM MES buffer (pH 5.5) containing ascorbic acid at a concentration of 2 mg/ml, in the presence or absence of aniline (100 mM). The reaction mixtures were incubated at ambient temperature for 30 or 60 min followed by analyses on a size-exclusion HPLC, using 30% CH_3CN in 50 mM ammonium acetate (pH 6.7) as eluant at a flow rate of 0.8 ml/min.

2.6. Synthesis of [^{18}F]FBA using 4-formyl-N,N,N-trimethylanilinium triflate as precursor

The radiolabeling of 4-formyl-*N*,*N*,*N*-trimethylanilinium triflate with F-18 was carried out using a GE FX_{F-N} module (shown in Fig. 1). Briefly, the bolus of ^{18}O-H_2O containing the ^{18}F was loaded onto a Chromafix 30-PS-HCO_3 ^{18}F separation cartridge and eluted into the graphite reaction vessel of the GE FX_{F-N} module with a solution of 5.7 mg Kryptofix K_{222}, 0.6 mg K_2CO_3 and 2 mg K_2SO_4 in 1 ml CH_3CN / water (0.6:0.4 v/v). The solvent was evaporated at 70°C at reduced pressure (~33 kPa) under an Ar stream for 5 min. Then, 1 ml of CH_3CN was added and evaporation resumed at 70°C for 3 min. After that, another 1 ml of CH_3CN was added and evaporation continued at 100°C for another 5 min. The Ar flow was stopped and the residue was dried at 100°C at reduced pressure (~8 kPa) for 5 min. After cooling to 60°C, a solution of 4-formyl-*N*,*N*,*N*-trimethylanilinium triflate (1.5–3.0 mg) in anhydrous DMSO (0.3 ml) was added. The reaction vessel was sealed, stirred and heated at 100°C for 10 min. Upon cooling to 40°C, the reaction mixture was diluted with 0.2% acetic acid (3.7 ml) and

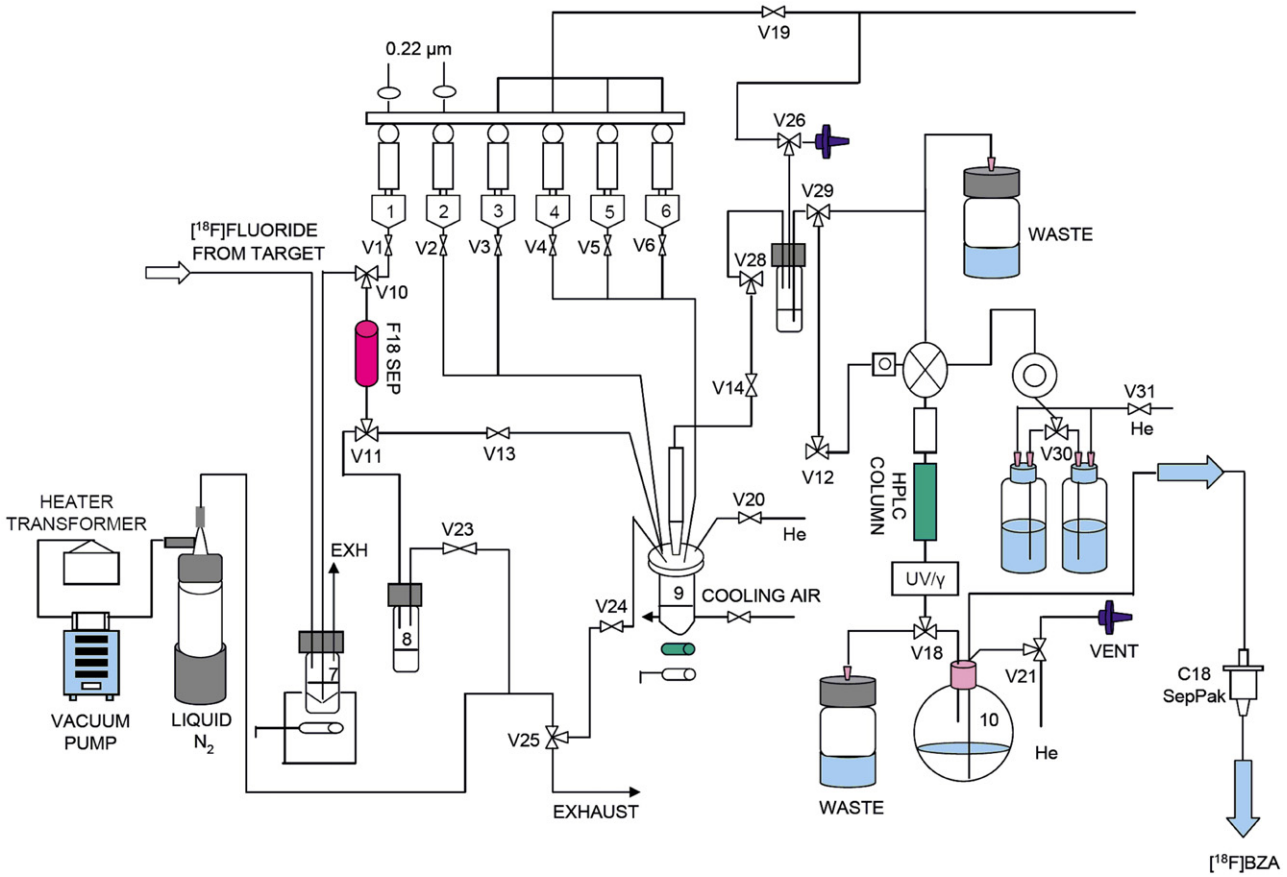

Fig. 1. Schematic diagram of the automated synthesis of [^{18}F]FBA using HPLC purification in a GE FXN module.

loaded onto a 250×10-mm, 10-µm semipreparative Gemini HPLC column, which was eluted with 30% CH_3CN/70% 0.2% acetic acid at a flow rate of 5 ml/min. The product peak was collected at 16.5–18 min and diluted with 50 ml of H_2O.

The well-mixed solution containing [^{18}F]FBA was then concentrated by passing through two tandemly connected classic C18 Sep-Pak columns and eluting components in three fractions (0.8, 1.0 and 1.0 ml, respectively) with 10 ml deionized water (DI water), followed by USP ethanol. The radioactivity in each fraction was measured in a dose calibrator, and the peak fraction containing the most radioactivity was used for the subsequent radiolabeling step of the exendin peptide. In general, 100–120 mCi of [^{18}F]FBA can be obtained.

2.7. Synthesis of [^{18}F]Ex(9–39) through formation of hydrazone

Exendin peptide (60 µg) was dissolved in 200 µl of 100 mM MES buffer (pH 5.5) containing aniline at a concentration of 100 mM and ascorbic acid at a concentration of 2 mg/ml. To this peptide solution was added 200–400 µl of [^{18}F]FBA in USP ethanol from the peak fraction. The well-mixed reaction mixture was incubated at room temperature for 30 min, followed by purification with a 1.5×10-cm Sephadex G-15 open column, using USP 1× PBS as an eluant. The fractions with peak radioactivity were collected and could be directly used for rodent imaging studies.

The product could also be purified by size-exclusion HPLC: the reaction mixture was diluted with 1 ml DI water and loaded onto a 300×10 mm Superdex peptide column and eluted with 30% CH_3CN/70% ammonium acetate (pH 6.7) at a flow rate of 0.8 ml/min. The product peak from the size-exclusion HPLC was collected at 16–20.5 min and diluted with 50 ml of H_2O. After being mixed well, the solution containing [^{18}F]-labeled peptide was formulated by passing through a classic C18 Sep-Pak column, followed by washing with 10 ml of DI water. The labeled peptide was then eluted with 2 ml 50%USP ethanol/50% saline into a dose vial for rodent imaging studies. Scheme 1 shows the synthesis of [^{18}F]FBA and [^{18}F]Ex(9–39).

2.8. Animals

Animals were maintained, treated, and cared for in compliance with guidelines of the Yale University's Institutional Animal Care and Use Committee (Yale's Assurance Number A3230-01). In vivo fluorescent imaging studies were performed in hairless SKH1 mice (Jackson

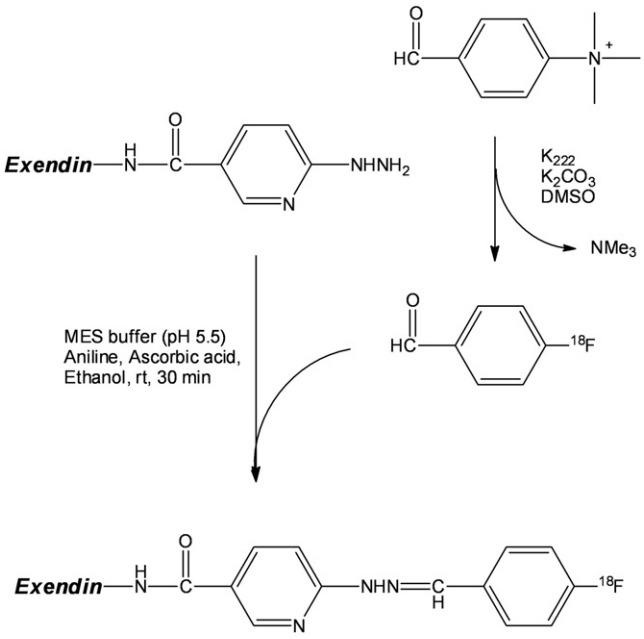

Scheme 1.

Laboratories, Bar Harbor, ME). Sprague–Dawley (~10 weeks of age) and BB-DP rats (three at 7weeks and three at 12 weeks) were used for PET imaging. Sprague–Dawley rats were divided into two groups. The first was a control cohort (n=4). The second was a diabetic group (n=6) scanned 24 to 72 h after β-cell death was chemically induced by treatment with streptozotocin (STZ: 65 mg in sterile saline administered by intraperitoneal injection).

2.9. Positron emission tomography imaging and analysis

After being anesthetized with isoflurane, animals were placed in temperature-regulated Plexiglas cylinders equipped to maintain and regulate anesthesia and to provide access to the tail for catheter placement. The aperture of the high-resolution research tomograph PET camera (Siemens/CTI, Knoxville, TN) was equipped with a custom-built insert to hold three cylinders symmetrically spaced for simultaneous imaging of three rats during each scan session. Each rat was injected intravenously via a tail vein with [^{18}F]Ex(9–39) (0.187±0.084 mCi) in a volume of 0.2 ml as a bolus injection over approximately 30 s. Immediately after infusion of radiotracer, the injection line was flushed with no more than 0.5 ml saline. Dynamic PET data were acquired in list mode for 180 to 240 min. Images were reconstructed using the MOLAR algorithm with corrections for attenuation, randoms, scatter, and dead time [25]. Regions of interest for pancreas, liver and kidney cortex were manually delineated on the PET images. Regional TACs were extracted from the dynamic PET images and converted to standardized uptake value (SUV) units by normalization for injected activity and animal body weight.

2.10. Measurement of pancreas insulin content

Animals were sacrificed immediately after imaging. The pancreas was removed and weighed, then placed in acid–ethanol (75% ethanol with 1.5% HCl) overnight to extract total insulin. The extract solutions were combined and centrifuged (13,000 rpm for 5 min at 4°C), and the supernatant was assayed for insulin content by radioimmunoassay (Linco, St. Louis, MO).

3. Results and discussion

3.1. β-Cell selectivity: In vitro cell binding assays using ^{125}I-exendin (9–39)

Normalized uptake and retention in the INS-1 cells (34.1±8.0 and 3.0±1.3) was significantly (P<.001) higher than in the PANC-1 cells (1.4±0.2 and 0.1±0.0). Thus, the specificity of ^{125}I-exendin (9–39) for the INS-1 cells was ~24 to 1 for uptake and ~30 to 1 for retention.

3.2. Molecular targeted fluorescent imaging of pancreatic BCM with exendin-4-Cy.5.5

The results from the binding assay of exendin-4-Cy.5.5 to the INS-1 (832/13) rat insulinoma cell line are shown in Fig. 2, indicating a specific and saturable binding of exendin to β-cell. The preferential localization of exendin-4-Cy5.5 to the pancreas was visualized by in vivo fluorescence imaging with exendin-4-Cy.5.5 and further confirmed in the excised tissue with a relative fluorescence intensity of pancreas to liver of ~5 to 1 (Fig. 3).

3.3. Coupling of FBA to HYNIC-functionalized exendin (9–39) peptide to prepare the nonradiolabeled test compound, F-19-exendin (9–39) peptide, as the reference

As cold runs, the FBA was conjugated to HYNIC-functionalized exendin peptide under different reaction conditions. The size-exclusion HPLC profiles of the reaction mixtures are shown in Fig. 4. The hydrazone has peak absorption at 360 nm; therefore, the absorbance at 360 nm

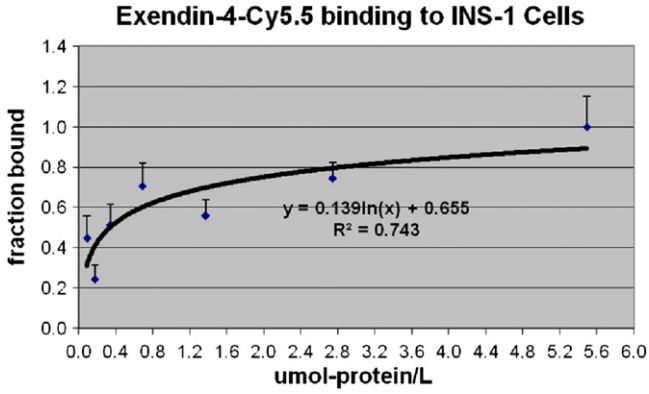

Fig. 2. Exendin-4-Cy5.5 binding to INS-1 (832/13) cells.

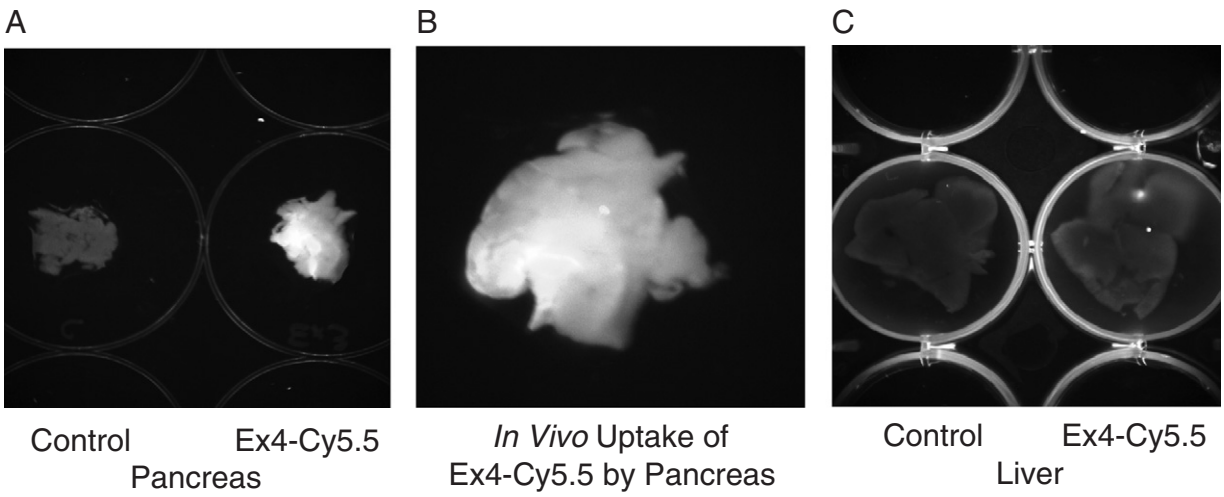

Fig. 3. (A) Fluorescence enhancement in pancreas of mouse after a bolus injection of approximately 40 nmol of exendin-4-Cy5.5 via an indwelling jugular catheter (right well) compared with pancreas of an untreated mouse. (B) Enlargement of exendin-4-Cy5.5-treated mouse pancreas from the image in (A). (C) Similar fluorescence intensity was observed in the liver of the control (left well) and the exendin-4-Cy5.5-treated mouse (right well). Tissue was excised 45 min after a bolus injection of exendin-4-Cy5.5

was used to monitor the formation of the hydrazone between FBA and HYNIC-functionalized exendin (9–39). The maximum absorption of FBA is not at 360 nm; however, the absorption is strong enough to monitor its disappearance in the reaction mixture.

Without the presence of aniline as catalyst, the conjugation reaction between FBA and HYNIC-functionalized exendin (9–39) was not efficient. Even though the reaction time was extended to 2 h (Fig. 4B), a large amount of unconjugated FBA (the peak at 28.52 min) still remained in the reaction mixture. In another run, the reaction temperature was elevated to 60°C for 2 h with no appreciable improvement (data not shown). However, when aniline was added at a concentration of 100 mM, the reaction was dramatically activated and no FBA was observed using size-exclusion HPLC analysis (curve C in Fig. 4). These results were consistent with previous reports [25–27].

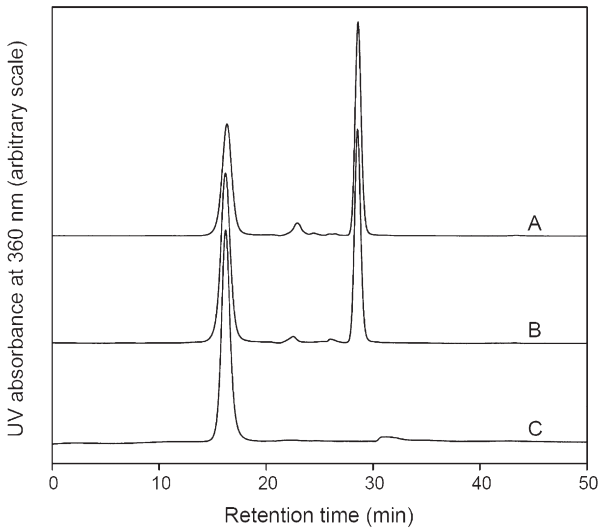

Fig. 4. 4-Fluorobenzaldehyde was conjugated to HYNIC-functionalized exendin (9–39) under different reaction conditions: (A) 30 μg of exendin (9–39) and 1.0 μg of FBA were dissolved in 200 μl of 100 mM MES buffer (pH 5.5) containing ascorbic acid at a concentration of 2 mg/ml and the reaction mixture was incubated at ambient temperature for 30 min; (B) the reaction conditions were the same as for (A) but the incubation time was 120 min; (C) 30 μg of exendin (9–39) and 1.0 μg of FBA were dissolved in 200 μl of 100 mM MES buffer (pH 5.5) containing 2 mg/ml ascorbic acid and 100 mM aniline. The reaction mixture was incubated at ambient temperature for 30 min. Aniline acted as catalyst for the coupling reaction.

3.4. Synthesis of [^{18}F]FBA

A typical reversed phase HPLC radiochromatogram of [^{18}F]FBA synthesized in this study is shown in Fig. 5B. For identification, the HPLC profile under identical condition of FBA as standard is also shown in Fig. 5A (254 nm). The column was Gemini-NX (Phenomenex), and the mobile phase was CH_3CN/water (30/70, v/v), with a flow rate of 2 ml/min. The 0.37-min difference between the UV and radioactivity peaks was due to the approximately 0.74-ml tubing volume between the respective detectors. [^{18}F]4-Fluorobenzaldehyde was routinely obtained with both the radioactivity purity and chemical purity more than 98%.

3.5. Radiolabeling of exendin (9–39) with [^{18}F]FBA

Fig. 6 shows a typical size-exclusion HPLC chromatograph of ^{18}F-radiolabeled exendin (9–39) after purified over a 1.5×10-cm open Sephadex G-15 column using PBS as the eluant. The UV signal was monitored at 360 nm since the hydrazone has maximum absorption at this wavelength. The peak at 26.0 min in the UV profile was due to PBS. The appearance of the UV peak 0.92 min earlier than the radioactivity peak was due to the approximately 0.74-ml tubing volume between the respective detectors. The ^{18}F-radiolabeled exendin (9–

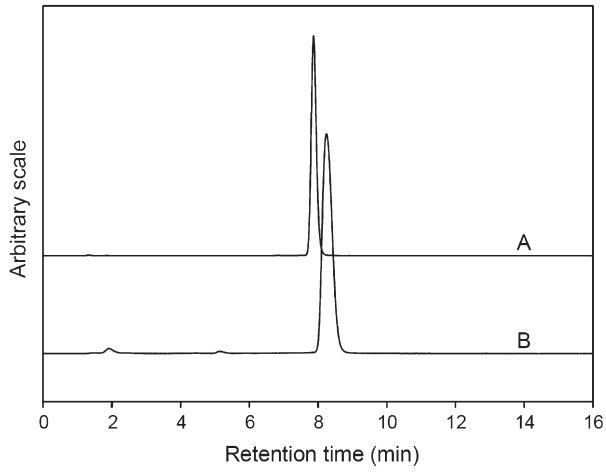

Fig. 5. Reversed phase HPLC analysis of [^{18}F]4-fluorobenzaldehyde. (A) HPLC UV profile of FBA as standard; (B) a typical HPLC radioactivity profile of [^{18}F]FBA synthesized in this study.

39) has the same retention time on the analytical size-exclusion HPLC as the nonradiolabeled test compound (F-19-exendin (9–39) peptide, prepared as described above in 2.5 and 3.3) (see Figs. 4 and Fig. 6). The radiochemical purity of the ^{18}F-radiolabeled exendin (9–39) was usually more than 95% based on the HPLC profile. The identity of the final ^{18}F-radiolabeled exendin (9–39) was further confirmed by coinjection of the reference compound, F-19-exendin (9–39) peptide, with an aliquot of the final product from the dose vial (data not shown). Typically, 4–10 mCi of radiolabeled peptide was obtained by this procedure. The specific radioactivity of the ^{18}F-radiolabeled peptide used in the animal studies was estimated to be ~600–700 mCi/μmol (at the end of synthesis) or ~1800–2100 mCi/μmol (corrected to EOB) by measuring the UV peak area at 254 nm in the HPLC profile and the injected radioactivity.

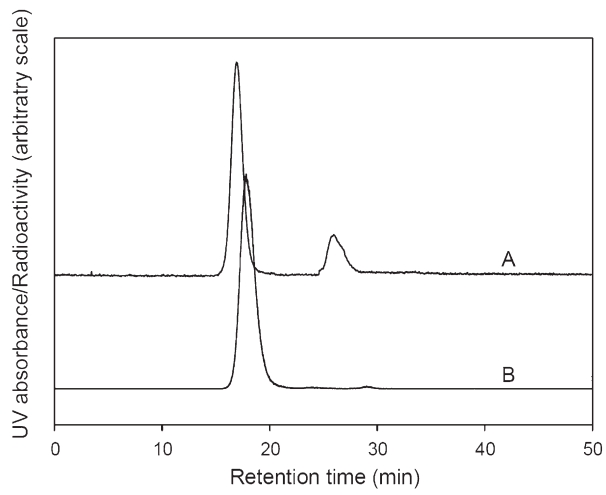

Fig. 6. Size-exclusion HPLC chromatography of ^{18}F-radiolabeled exendin (9–39). The radiolabeled peptide was purified on an open G-15 column using USP PBS as eluant. (A and B) UV and radioactivity HPLC profiles, respectively, of the radiolabeled peptide. The peak at 26.0 min in UV profile was due to the presence of PBS in the product solution.

3.6. GLP-1R imaging with PET

A representative PET image of an SD rat at 10–30 min postinjection of [^{18}F]Ex(9–39) is shown in Fig. 7. High concentration of radioactivity was observed in the myocardium and kidney. The uptake in pancreas was low and not appreciably different than surrounding tissues with lower expression of the GLP-1R.

Time–activity curves for the pancreas, liver and kidney are shown in Fig. 8. As shown, the pancreatic SUV peaked at about 10 min and plateaued after 50 min. No apparent difference in the pancreatic uptake of [^{18}F]Ex(9–39) was observed among the control, STZ-induced diabetic and BB-DP rats. In addition, there was no apparent correlation between pancreatic SUVs and postmortem measures of insulin content, as shown in Fig. 9.

The Fig. 6 and TAC of the [^{18}F]Ex(9–39) is the inverse of that which we observed recently in our evaluation of [^{11}C]DTBZ and [^{18}F]FP-DTBZ to successfully image BCM in rats. In that study, uptake of [^{11}C]DTBZ and [^{18}F]FP-DTBZ by the liver and pancreas rose to a plateau within 15 min, whereas the kidney activity quickly spiked then decreased to a substantially lower level [28]. In agreement with the earlier studies with [^{11}C]DTBZ [29,30], we observed a decrease in pancreas uptake of [^{11}C]DTBZ and [^{18}F]FP-DTBZ that correlated with loss of insulin-positive islet area from immunohistochemistry analysis and total insulin content [28]. Recent studies, however, suggest that the VMAT2 expression is tissue-specific and that while VMAT2 is expressed in human and pig islets, it is not found in rat and mouse islets. Nevertheless, a significant correlation of radiolabeled DTBZ and FP-DTBZ with pancreatic BCM in rats

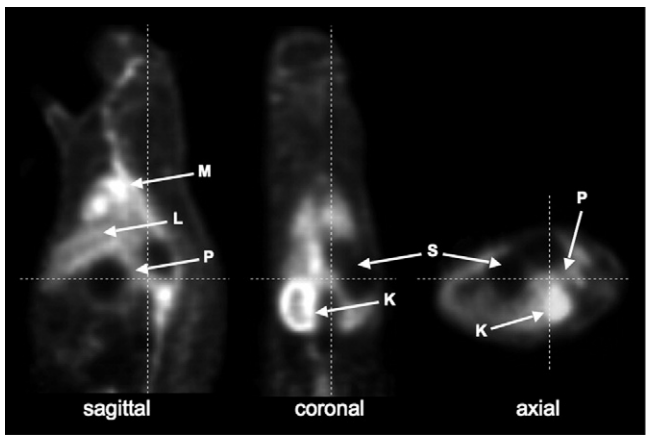

Fig. 7. Positron emission tomography image of an SD control rat at 10–30 min after injection of [^{18}F]Ex(9–39). K=kidney, L=liver, M=myocardium, P=pancreas, S=stomach.

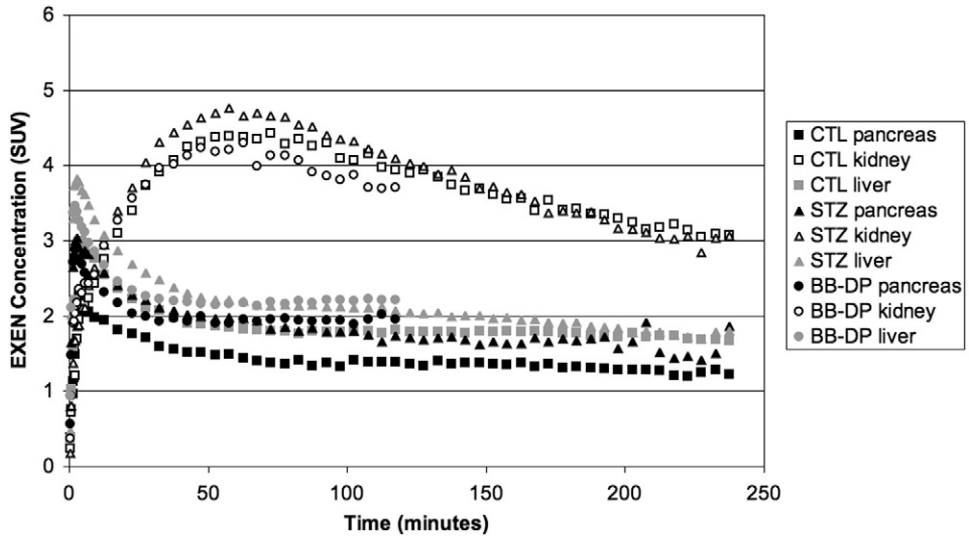

Fig. 8. [^{18}F]Ex(9–39) TACs for pancreas, liver and kidney in control (CTL), STZ and BB-DP rats.

was established by us and others. While a large fraction of pancreatic binding was found to be nonspecific, our studies indicated that a substantial fraction of the [^{18}F]FP-DTBZ binding was displaceable in vivo. Taken together, these results suggest that a specific DTBZ binding target exists in the rat and mouse pancreas that decreases with the loss of pancreatic BCM. Thus, the lack of correlation of pancreatic uptake of [^{18}F]Ex(9–39) with pancreatic insulin content and BCM cannot be ascribed to methodologically deficiencies.

Site-specific labeling of biomolecules is always desired, especially in cases where the biomolecules to be labeled have multiple sites capable of being labeled (such as multiple primary amine groups), which would result in a mixture of labeled compounds. For proteins, especially peptides, the primary amine groups on lysine residues within the sequences usually play critical roles in exerting proper bioactivities. Once these amine groups are blocked by tags, such as radiolabeled chelators or fluorescent groups, the bioactivities of the labeled molecules would be either impaired or completely lost.

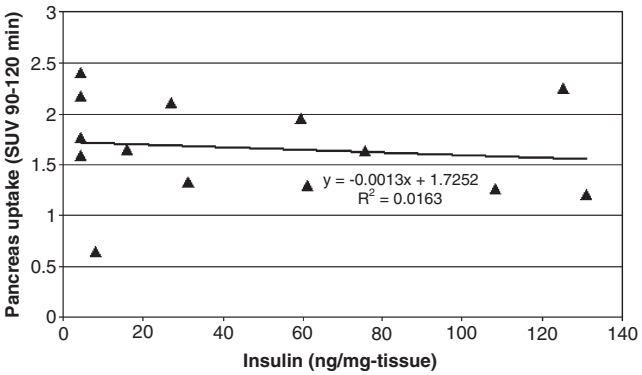

Fig. 9. Relationship between [^{18}F]Ex(9–39) SUV in pancreas and postmortem measures of islet insulin content.

The formation of hydrazones as an effective way to label biomolecules has been widely used in radiolabeling of oligonucleotides, proteins and peptides for SPECT imaging [31–33]. The reaction between benzaldehyde and hydrazine groups is specific and the resulting hydrazone bond is stable under physiological conditions; by using this approach, biomolecules can be labeled in a site-specific manner.

Exendin (9–39) is a truncated version of exenatide and an antagonist of GLP-1R and it can also be a potential agent for GLP-1R imaging. Exendin (9–39) has three primary amine groups; one each at the N-terminus, at Lys12, and at Lys27. In this study, the F-18 was introduced specifically to Lys27.

To complete the entire synthesis procedure, a GE FX_{F-N} module was connected to a semiautomatic hot cell. The synthesis of [^{18}F]FBA was performed in the GE FX_{F-N} module. After semipreparative HPLC purification, [^{18}F]FBA was collected in a bottle containing 50 ml DI water. The well-mixed solution was then transferred to the semiautomatic module by passing through two tandemly connected classic C18 Sep-Pak cartridges. The rest of the synthesis was performed as described in the Methods and Materials section using a semiautomatic hot cell.

Good yields have been reported when using the hydrazone formation method to label proteins with F-18 [34]; however, as shown in Fig. 4, we found that, at a molar ratio of ~1:1, the yield of the desired product was low even after the reaction time was extended to 2 h, which was evidenced by the existence of a large amount of unreacted FBA. A similar result was obtained from a test radiosynthesis using the same conditions (data not shown). When aniline was added to a final concentration of 100 mM, no free FBA was observed based on the HPLC analysis after 30 min of incubation, suggesting that aniline is required for efficient labeling. The addition of aniline did not affect the quality/purity of the

product since it could be easily removed by size-exclusion HPLC or open-column size-exclusion chromatography. Based on the quality of our final ^{18}F-radiolabeled exendin (9–39) (Fig. 6), we demonstrate that the synthetic procedure described here is an efficient and reliable method to provide a site-specifically F-18-labeled peptide.

With the site-specific F-18-labeled [^{18}F]Ex(9–39) in hand, PET imaging studies in rodents were successfully carried out. The results showed that [^{18}F]Ex(9–39) appeared to accumulate in several organs, including the pancreas, during early time frames after administration. [^{18}F]Ex(9–39) exhibited highest uptakes in kidneys, suggesting that clearance through the kidney may be the major metabolic pathway for [^{18}F]Ex(9–39). The relatively lower uptakes in pancreas and the lack of any significant differences in SUVs between control and diabetic rats suggest that there is no specific binding of [^{18}F]Ex(9–39) to the GLP-1Rs in pancreas. Furthermore, the correlation of pancreatic SUVs with postmortem measures of insulin content was poor (R^2=.0163). Thus, we conclude that the [^{18}F]Ex(9–39) peptide labeled at Lys27 is not a promising biomarker for imaging the BCM.

Despite previous reports that the modification at the ε-amine of Lys27 should not compromise the binding affinity of exendin-4 to GLP-1R [20–22], it appears that, in our case, the addition of a [^{18}F]FBA and a HYNIC group to Lys27 led to a change in binding affinity of the peptide, although we have not tested its in vitro affinity. From analysis of the crystal structure of exendin-4 (9–39) in complex with nGLP-1R, Runge et al. [35] reported that Lys27 of exendin (9–39) forms a salt bridge with Glu127 of nGLP-1R and Glu24 of itself; in addition, the backbone carbonyl of Lys27 of exendin (9–39) forms a hydrogen bond with the side chain of Arg121 of nGLP-1R. Therefore, a reasonable explanation for the absence of specific binding in our case could be the introduction of a bulky hydrophobic moiety at Lys27 with [^{18}F]-FBA and HYNIC tags that interferes with its binding to the GLP-1R. We hypothesize therefore that modification of the Lys12 or the terminal amino group will have less or minimal impact on the binding affinity of the modified exendin-4 with GLP-1R. However, to confirm this hypothesis, further BCM imaging studies are needed using [^{18}F]Ex(9–39) with modifications on amino acid residues other than Lys27.

4. Conclusion

Exendin (9–39) was readily radiolabeled with F-18 in a site-specific manner by using the formation of a hydrazone between HYNIC tagged Lys27 and [^{18}F]FBA. Aniline acted as a catalyst for the formation of the hydrazone and was required for efficient labeling. Introduction of [^{18}F]FBA to the HYNIC-modified Lys27 residue might lead to a change in binding affinity, as seen by the absence of specific binding to the GLP-1R in pancreas. Preparation of [^{18}F]exendin analogues with the F-18 label at sites other than Lys27, especially on the C-terminal of the peptide, may improve its potential as an imaging probe for the BCM.

Supplementary materials related to this article can be found online at doi:10.1016/j.nucmedbio.2011.07.011.

Acknowledgments

The authors thank the staff of the Yale University PET Center for their technical expertise and support. Funding for this study was provided by the Juvenile Diabetes Research Foundation (JDRF) and Yale Pfizer Bioimaging Alliance. This publication was also made possible by CTSA Grant Number UL1 RR024139 from the National Center for Research Resources (NCRR), a component of the National Institutes of Health (NIH) and NIH roadmap for Medical Research. Its contents are solely the responsibility of the authors and do not necessarily represent the official view of NCRR or NIH.

References

[1] Reubi JC, Waser B. Concomitant expression of several peptide receptors in neuroendocrine tumours: molecular basis for in vivo multireceptor tumour targeting. Eur J Nucl Med Mol Imaging 2003;30:781–93.
[2] Körner M, Stökli M, Waser B, Reubi JC. GLP-1 receptor expression in human tumors and human normal tissues: potential for in vivo targeting. J Nucl Med 2007;48:736–43.
[3] Vilsbøll T, Agersø H, Krarup T, Holst JJ. Similar elimination rates of glucagon-like peptide-1 in obese type 2 diabetic patients and healthy subjects. J Clin Endocrinol Metab 2003;88:220–4.
[4] Barnett A. DPP-4 inhibitors and their potential role in the management of type 2 diabetes. Int J Clin Pract 2006;60:1454–70.
[5] Eng J, Kleinman WA, Singh L, Singh G, Raufman JP. Isolation and characterization of exendin-4, an exendin-3 analogue, from *Heloderma suspectum* venom. Further evidence for an exendin receptor on dispersed acini from guinea pig pancreas. J Biol Chem 1992;267:7402–5.
[6] Cvetković RS, Plosker GL. Exenatide: a review of its use in patients with type 2 diabetes mellitus (as an adjunct to metformin and/or a sulfonylurea). Drugs 2007;67:935–54.
[7] Holst JJ. Pharmacology of GLP-1-based therapies. Br J Diabetes Vasc Dis 2008;8:S10–8.
[8] Göke R, Fehmann HC, Linn T, Schmidt H, Krause M, Eng J, et al. Exendin-4 is a high potency agonist and truncated exendin-(9–39)-amide an antagonist at the glucagon-like peptide 1-(7–36)-amide receptor of insulin-secreting β-cells. J Biol Chem 1993;268:19650–5.
[9] Wicki A. [Lys40(Ahx-DTPA-111In)NH_2]-Exendin-4 is a highly efficient radiotherapeutic for glucagon-like peptide-1 receptor-targeted therapy for insulinoma. Clin Cancer Res 2007;13:3696–705.
[10] Wild D, Béhé M, Wicki A, Storch D, Waser B, Gotthardt M, et al. [Lys40(Ahx-DTPA-111In)NH_2]Exendin-4, a very promising ligand for glucagon-like peptide-1 (GLP-1) receptor targeting. J Nucl Med 2006;47:2025–33.
[11] Christ E, Wild D, Forrer F, Brandle M, Sahli R, Clerici T, et al. Glucagon-like peptide-1 receptor imaging for localization of insulinomas. J Clin Endocrinol Metab 2009;94:4398–405.

[12] Wild D, Mäcke H, Christ E, Gloor B, Reubi JC. Glucagon-like peptide 1-receptor scans to localize occult insulinomas. N Engl J Med 2008;359:766–8.
[13] Wild D, Wicki A, Mansi R, Béhé M, Keil B, Bernhardt P, et al. Exendin-4-based radiopharmaceuticals for glucagonlike peptide-1 receptor PET/CT and SPECT/CT. J Nucl Med 2010;51:1059–67.
[14] Fehmann HC, Jiang J, Schweinfurth J, Wheeler MB, Boyd III AE, Göke B. Stable expression of the rat GLP-I receptor in CHO cells: activation and binding characteristics utilizing GLP-I(7–36)-amide, oxyntomodulin, exendin-4, and exendin(9–39). Peptides 1994;15:453–6.
[15] Mukai E, Toyoda K, Kimura H, Kawashima H, Fujimoto H, Ueda M, et al. GLP-1 receptor antagonist as a potential probe for pancreatic β-cell imaging. Biochem Biophys Res Commun 2009;389:523–6.
[16] Cline GW, Carson RE, Ding YS, Huang H, Weinzimmer DP, Jakowski A, et al. Islet-selectivity of G-protein coupled receptor (GPCR) ligands evaluated for PET imaging. Diabetes 2008;57(Suppl 1):A47.
[17] Gotthardt M, Fischer M, Naeher I, Holz JB, Jungclas H, Fritsch HW, et al. Use of the incretin hormone glucagon-like peptide-1 (GLP-1) for the detection of insulinomas: initial experimental results. Eur J Nucl Med 2002;29:597–606.
[18] Aspinwall S, McLaughlin W, Vizard D, Cline G. Molecular targeted fluorescent imaging of pancreatic beta-cell mass. 5th Annual Meeting of The Society for Molecular Imaging; 2006, pp. 132.
[19] Kimura H, Ogawa Y, Kawashima H, Mukai E, Toyoda K, Fujimoto H, et al. Development of in vivo imaging agents targeting glucagon-like peptide-1 receptor (GLP-1R) in pancreatic islets. J Nucl Med 2009;50(Suppl 2):326.
[20] Jin CH, Chae SY, Son S, Kim TH, Um KA, Youn YS, et al. A new orally available glucagon-like peptide-1 receptor agonist, biotinylated exendin-4, displays improved hypoglycemic effects in db/db mice. J Control Release 2009;133:172–7.
[21] Son S, Chae SY, Kim CW, Choi YG, Jung SY, Lee S, et al. Preparation and structural, biochemical, and pharmaceutical characterizations of bile acid-modified long-acting exendin-4 derivatives. J Med Chem 2009;52:6889–96.
[22] Chae SY, Jin CH, Shin JH, Son S, Kim TH, Lee S, et al. Biochemical, pharmaceutical and therapeutic properties of long-acting lithocholic acid derivatized exendin-4 analogs. J Control Release 2010;142: 206–13.
[23] Sweet IR, Cook DL, Lernmark A, Greenbaum CJ, Wallen AR, Marcum ES, et al. Systematic screening of potential β-cell imaging agents. Biochem Biophys Res Commun 2004;;314:976–83.
[24] Haka MS, Kilbourn MR, Watkins GL, Toorongian SA. Aryltrimethylammonium trifluoromethanesulfonates as precursors to aryl [^{18}F] fluorides: improved synthesis of [^{18}F]GBR-13119. J Labelled Compd Radiopharm 1989;27:823–38.
[25] Carson RE, Barker WC, Liow JS, Johnson CA. Design of a motion compensation OSEM list-mode algorithm for resolution–recovery reconstruction for the HRRT. IEEE Nucl Sci Symp Conf Rec 2003: 3281–5.
[26] Dirksen A, Dawson PE. Rapid oxime and hydrazone ligations with aromatic aldehydes for biomolecular labeling. Bioconjug Chem 2008;19:2543–8.
[27] Dirksen A, Dirksen S, Hackeng TM, Dawson PE. Nucleophilic catalysis of hydrazone formation and transimination: implications for dynamic covalent chemistry. J Am Chem Soc 2006;128:15602–3.
[28] Singhal T, Ding YS, Weinzimmer D, Normandin MD, Labaree D, Ropchan J, et al. Pancreatic β-cell mass PET imaging and quantification using [^{11}C]DTBZ and [^{18}F]FP-(+)-DTBZ in rodent models of diabetes. Mol Imaging Biol 2010 (in press) PMID 20824509.
[29] Souza F, Simpson N, Raffo A, Saxana C, Maffei A, Hardy M, et al. Longitudinal noninvasive PET-based β cell mass estimates in a spontaneous diabetes rat model. J Clin Invest 2006;116:1506–13.
[30] Simpson NR, Souza F, Witkowski P, Maffei A, Raffo A, Herron A, et al. Visualizing pancreatic β-cell mass with [^{11}C]DTBZ. Nucl Med Biol 2006;33:855–64.
[31] He J, Wang Y, Dou S, Liu X, Zhang S, Liu G. Affinity enhancement pretargeting: synthesis and testing of a ^{99m}Tc-labeled bivalent MORF. Mol Pharmacol 2010;7:1118–24.
[32] Harris TD, Sworin M, Williams N, Rajopadhye M, Damphousse PR, Glowacka D, et al. Synthesis of stable hydrazones of a hydrazinonicotinyl-modified peptide for the preparation of ^{99m}Tc-labeled radiopharmaceuticals. Bioconjug Chem 1999;10:808–14.
[33] He J, Liu G, Dou S, Gupta S, Rusckowski M, Hnatowich D. An improved method for covalently conjugating morpholino oligomers to antitumor antibodies. Bioconjug Chem 2007;18:983–8.
[34] Chang YS, Jeong JM, Lee YS, Kim HW, Rai GB, Lee SJ, et al. Preparation of ^{18}F-human serum albumin: a simple and efficient protein labeling method with ^{18}F using a hydrazone-formation method. Bioconjug Chem 2005;16:1329–33.
[35] Runge S, Thøgersen H, Madsen K, Lau J, Rudolph R. Crystal structure of the ligand-bound glucagon-like peptide-1 receptor extracellular domain. J Biol Chem 2008;283:11340–7.